

# Psi-Net: Shape and boundary aware joint multi-task deep network for medical image segmentation

Balamurali Murugesan<sup>1,2\*</sup>, Kaushik Sarveswaran<sup>2,3\*†</sup>, Sharath M Shankaranarayana<sup>4</sup>,  
Keerthi Ram<sup>2</sup>, and Mohanasankar Sivaprakasam<sup>1,2</sup>

**Abstract**—Medical image segmentation is a primary task in many applications, and the accuracy of the segmentation is a necessity. Recently, many deep learning networks derived from U-Net have been extensively used and have achieved notable results. To further improve and refine the performance of U-Net, parallel decoders along with mask prediction decoder have been carried out and have shown significant improvement with additional advantages. In our work, we utilize the advantages of using a combination of contour and distance map as regularizers. In turn, we propose a novel architecture Psi-Net with a single encoder and three parallel decoders, one decoder to learn the mask and other two to learn the auxiliary tasks of contour detection and distance map estimation. The learning of these auxiliary tasks helps in capturing the shape and boundary. We also propose a new joint loss function for the proposed architecture. The loss function consists of a weighted combination of Negative likelihood and Mean Square Error loss. We have used two publicly available datasets: 1) Origa dataset for the task of optic cup and disc segmentation and 2) Endovis segment dataset for the task of polyp segmentation to evaluate our model. We have conducted extensive experiments using our network to show our model gives better results in terms of segmentation, boundary and shape metrics.

## I. INTRODUCTION

Image segmentation is the process of delineating structures of importance from an image. Identifying these structures in the medical image finds application in many medical procedures. To state some of them: 1) segmentation of optic cup and disc in the retinal fundus image is useful in glaucoma screening, 2) segmentation of polyp in colonoscopy image is helpful in cancer diagnosis, 3) segmentation of the organ, bones benefit surgery planning and 4) segmentation of lung nodules in chest computed tomography aids physicians to differentiate malignant lesions from benign lesions. In recent years, deep learning networks [1] are widely used in medical image segmentation, and the most commonly used deep learning network is UNet [2].

UNet [2] is an encoder-decoder type of network which takes an image as input and outputs a pixel-wise classification probability score with cross-entropy as its loss function. This network has set new state of the art results for different medical image segmentation tasks. But there are some drawbacks with the architecture type, and loss functions

used. For instance, the encoder block of the network under-samples the input through max-pooling layers which results in loss of spatial information. Similarly, having pixel-wise classification alone as a loss function produces uneven mask boundaries and outliers. In addition to this, the loss function doesn't take shape information into account which can help in performance improvement. Also, using cross-entropy as a loss function introduces class imbalance problem for images in which background dominates the object of interest which is very common in the medical images. To overcome the above-mentioned issues, multiple works have been reported in the literature [5], [6], [7], [8]. In that, the architecture and loss functions followed by [3] and [4] are of our interest. Both these works use a similar architecture with a single encoder and two parallel decoders. The decoders are used for mask and contour prediction in [3] whereas in [4] it is used for estimating mask and distance map. Contour and distance map estimation act as regularizers to mask prediction. Shape information is imposed through contour and distance map in [3] and [4]. Class imbalance problem is mitigated in [4] through its joint classification and regression approach while it will still be an issue in [3] because of both decoders acting as classifiers. The boundaries obtained using [4] are smooth and the segmentation has reduced outliers compared to [2], [3]. But in multi-instance object segmentation cases, an object of smaller size can be treated as an outlier resulting in unsatisfactory segmentation. The summary of the above discussion are shown in Table I.

The main contributions of our paper are as follows:

- We propose a novel multi-task network Psi-Net with a single encoder and three decoders. The decoders are used to learn three different tasks in parallel. The mask prediction is the primary task while the contour detection and distance map estimation are auxiliary tasks. These additional tasks are used to regularize the mask prediction path to produce a refined mask with smooth boundaries.
- We propose a novel joint loss function to handle the

TABLE I

SUMMARY OF PROS AND CONS OF THE MODELS.

	[2]	[3]	[4]	Ours
Shape information	x	✓	✓	✓
Class imbalance	x	x	✓	✓
Smooth boundary	x	x	✓	✓
Multiple object instances	✓	✓	x	✓

\* Contributed equally

† Work was done while interning at HTIC

<sup>1</sup> Indian Institute of Technology Madras (IITM), India

<sup>2</sup> Healthcare Technology Innovation Centre (HTIC), IITM, India

<sup>3</sup> Indian Institute of Information Technology Design & Manufacturing  
Kancheepuram (IIITDM), India

<sup>4</sup> Zasti, India

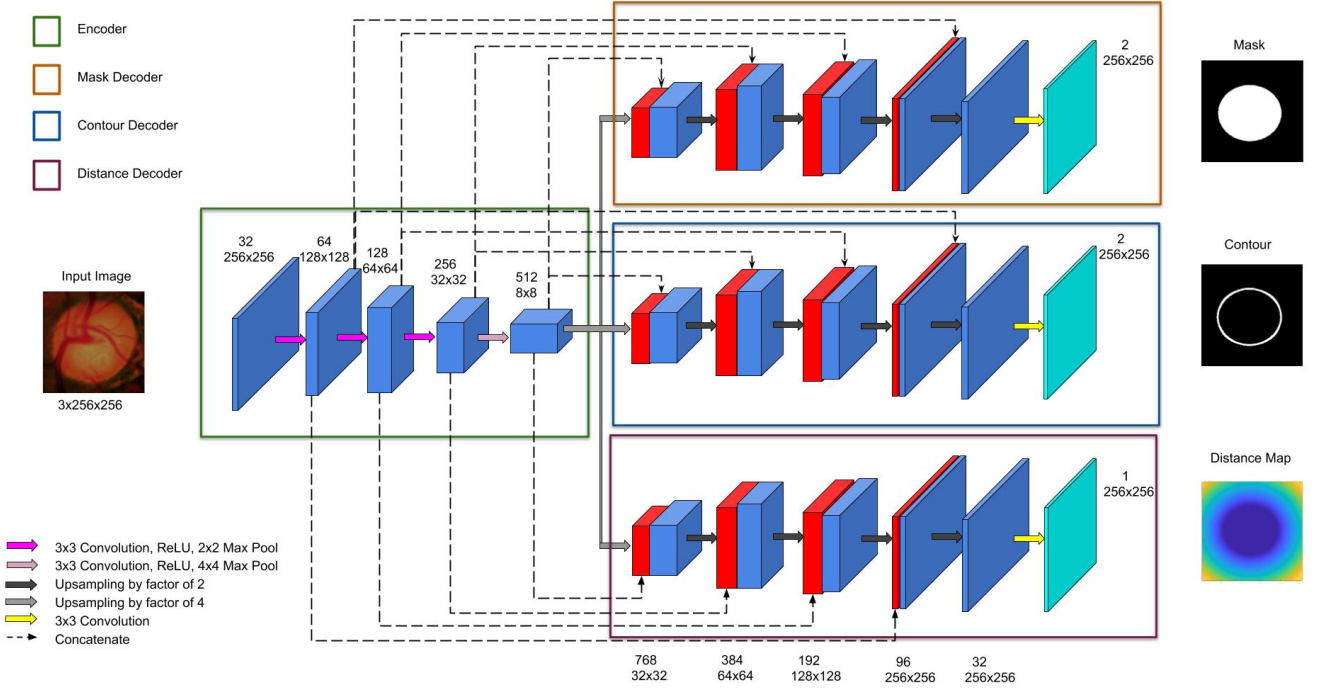


Fig. 1. Psi-Net: Proposed architecture for segmentation with a single encoder and three decoders.

three different tasks together. The joint loss function consists of a combination of Negative Log Likelihood (NLL) for mask, Negative Log Likelihood (NLL) for contour, and Mean Square Error (MSE) for distance.

- We qualitatively compared our results with [2], [3] and [4]. The following evaluation metrics are used to perform a quantitative comparison:
  - *Segmentation metrics* : Jaccard and Dice coefficients.
  - *Shape similarity metrics* : Hausdorff distance
  - *Boundary metrics* : Segmentation evaluation around boundaries using trimap method.

The comparative study showed that our network performed better than others in all the evaluation metrics producing a better mask with smooth boundaries.

## II. METHODOLOGY

### A. Architecture

The architecture Psi-Net is a UNet-like encoder-decoder network, with one contracting encoder path on the left and three expansive structurally similar decoder paths on the right. The encoder path consists of repeated downsampling operations which halves the size of feature map at each stage. Each downsampling operation is preceded by a convolution operation with kernel size 3x3 and stride 1, which is followed by a Rectified Linear Unit (ReLU) activation. Each decoder block is symmetric to the encoder, and at each decoder layer, the features from the corresponding encoder layer are concatenated which helps in retaining multi-scale features.

The final convolutional layer in the encoder is upsampled by a factor of 4 and given as input to the decoder blocks.

Each decoder block is trained for a different task - Mask segmentation, contour extraction and distance map estimation. The former two are pixel-wise classification tasks while the latter is a regression task. The blocks are identical in structure until the last layer, where a 3x3 convolution is applied, and the number of output channels is 1 in the distance decoder block and is equal to the number of input classes in the other two blocks. The outline of proposed network is shown in Fig. 1.

### B. Loss Function

The loss function consists of three components - Negative Log Likelihood (NLL) loss for mask and contour decoder blocks, and Mean Square Error (MSE) loss for the distance decoder block. Mask prediction is regularized by both contour and distance map predictions. The total loss is given by

$$\mathcal{L}_{total} = \lambda_1 \mathcal{L}_{mask} + \lambda_2 \mathcal{L}_{contour} + \lambda_3 \mathcal{L}_{distance} \quad (1)$$

where  $\lambda_1, \lambda_2, \lambda_3$  are scaling factors.

The individual losses are formulated below.

1) *Mask*:

$$\mathcal{L}_{mask} = \sum_{\mathbf{x} \in \Omega} \log p_{mask}(\mathbf{x}; l_{mask}(\mathbf{x})) \quad (2)$$

$\mathcal{L}_{mask}$  denotes the pixel-wise classification error.  $\mathbf{x}$  is the pixel position in image space  $\Omega$ .  $p_{mask}(\mathbf{x}; l_{mask})$  denotes the predicted probability for true label  $l_{mask}$  after softmax

activation function.

## 2) Contour:

$$\mathcal{L}_{contour} = \sum_{\mathbf{x} \in \Omega} \log p_{contour}(\mathbf{x}; l_{contour}(\mathbf{x})) \quad (3)$$

$\mathcal{L}_{contour}$  denotes the pixel-wise classification error.  $p_{contour}(\mathbf{x}; l_{contour})$  denotes the predicted probability for true label  $l_{contour}$  after softmax activation function.

## 3) Distance:

$$\mathcal{L}_{distance} = \sum_{\mathbf{x} \in \Omega} (\hat{D}(\mathbf{x}) - D(\mathbf{x}))^2 \quad (4)$$

$\mathcal{L}_{distance}$  denotes the pixel-wise mean square error.  $\hat{D}(\mathbf{x})$  is the estimated distance map after sigmoid activation function while  $D(\mathbf{x})$  is the ground-truth distance map.

# III. EXPERIMENTS AND RESULTS

## A. Dataset and Pre-processing

1) *Dataset Description:* We validated our proposed segmentation approach for the following two applications:

- 1) **Optic cup and disc segmentation** : We use ORIGA dataset [9] for the task of optic disc and cup segmentation. The dataset consists of 650 color fundus image with ground truth segmentations for optic disc and cup. The color fundus images are of dimension  $256 \times 256$ . Ellipse fit is applied to output segmentation mask.
- 2) **Polyp segmentation** : We also use Polyp segmentation dataset from MICCAI 2018 Gastrointestinal Image ANalysis (GIANA) [10]. The dataset consists of 912 images with ground truth masks. The dataset is split into 70% for training and 30% for testing. The images are center cropped and resized to  $256 \times 256$ .

2) *Preprocessing:* The dataset contains only segmentation mask. But for training our model, we need ground truth contour and distance map. The contour map is obtained by estimating the boundaries of connected components. These boundaries are subsequently dilated with a disk filter of radius 5. The distance map is obtained by applying an euclidean distance transform to the mask. The final distance map will contain zeros in the mask region, with the rest of the pixels denoting the shortest distance between that pixel and the mask boundary.

## B. Implementation Details

All the models are implemented using PyTorch. Models are trained for 150 epochs using Adam optimizer, with a learning rate of  $1e-4$  and batch size 4. Experiments have been conducted with NVIDIA GeForce GTX 1060 GPU - 6GB RAM.

## C. Evaluation metrics

1) *Segmentation evaluation:* Jaccard index and Dice similarity score are the most commonly used evaluation metrics for segmentation. Jaccard index (also known as intersection over union, IoU) is defined as the size of the intersection divided by the size of the union of the sample sets, and it is calculated as follows:

$$Jaccard(A, B) = \frac{|A \cap B|}{|A \cup B|} \quad (5)$$

where A corresponds to the output of the method and B to the actual ground truth.

DICE similarity score is a statistic also used for comparing the similarity of two samples. It is calculated as follows:

$$Dice(X, Y) = \frac{2|X \cap Y|}{|X| + |Y|} \quad (6)$$

where X and Y correspond, respectively, to the output of the method and the ground truth image.

2) *Shape Similarity:* The shape similarity is measured by using the Hausdorff distance between the shape of segmented object and that of the ground truth object, defined as

$$H(G, S) = \max \left\{ \sup_{x \in G} \inf_{y \in S} \|x - y\|, \sup_{y \in S} \inf_{x \in G} \|x - y\| \right\} \quad (7)$$

where G and S correspond, respectively, to the output of the method and the ground truth image.

## D. Results and Discussion

Some of the results obtained using our proposed model are depicted in Fig. 2. Some of the abbreviations which will be used in this section are Encoder (Enc), Decoder (Dec), Mask (M), Contour (C) and Distance (D). The results of the proposed network (1Enc 3Dec MCD) is compared with the following networks.

- A network (1Enc 1Dec M) [2] with a single encoder and a decoder having NLL as loss function for mask prediction.
- A network (1Enc 2Dec MC) [3] with a single encoder and two decoders having NLL as loss function for both mask and contour estimation.
- A network (1Enc 2Dec MD) [4] with a single encoder and two decoders having NLL as loss function for mask and MSE as loss function for distance map estimation.

1) *Standard Evaluation:* From Table II it can be seen that the network 1Enc 3Dec MCD has shown better performance compared to the networks 1Enc 1Dec M, 1Enc 2Dec MC and 1Enc 2Dec MD. This improvement in performance can be attributed to the use of two auxiliary regularizers, in the form of contour detection and distance map estimation, as opposed to a single regularizer in 1Enc 2Dec MC and 1Enc 2Dec MD. Both the networks 1Enc 2Dec MC and 1Enc 2Dec MD use shape information for mask refinement. While 1Enc 2Dec MD provides smooth boundaries compared to 1Enc 2Dec MC, it has a drawback in handling multiple object instances which is not an issue in 1Enc 2Dec MC. Since both these networks complement one another, combining

TABLE II  
COMPARISON OF SEGMENTATION AND SHAPE METRICS.

Architecture	Cup		Disc		Polyp		
	Dice	Jaccard	Dice	Jaccard	Dice	Jaccard	Hausdorff
1Enc 1Dec M [2]	0.8655	0.7712	0.9586	0.9215	0.8125	0.7323	24.133
1Enc 2Dec MC [3]	0.8715	0.7803	0.9646	0.9324	0.8151	0.7391	22.737
1Enc 2Dec MD [4]	0.8723	0.7807	0.9665	0.9358	0.8283	0.7482	22.686
1Enc 3Dec MCD (Ours)	<b>0.8745</b>	<b>0.7848</b>	<b>0.9667</b>	<b>0.9359</b>	<b>0.8462</b>	<b>0.7721</b>	<b>21.143</b>

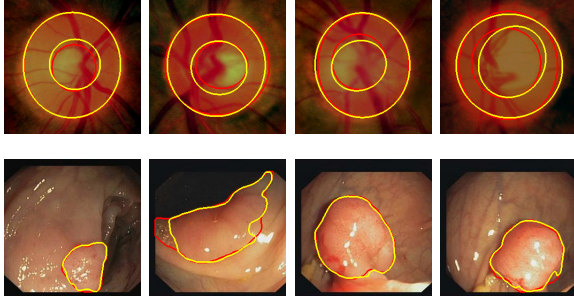


Fig. 2. Sample results, Red - Ground truth, Yellow - Predicted

these models brings the best result. The segmentation of polyp is relatively difficult when compared to optic cup and disc segmentation because of its large variations in size and shape. From Table II, it is evident that our network shows substantial improvement in performance for polyp segmentation compared to optic cup and disc segmentation.

2) *Shape Similarity*: Along with better segmentation, the network should also produce segmentation maps which are similar to ground truth masks regarding shape [3]. This shape similarity is obtained by Hausdorff distance. From Table II, it is clear that our network does well in capturing shape information compared to other networks. Also, sorting the Hausdorff distance helps in coming to the following inferences: 1) the addition of auxiliary tasks does help in preserving shape. 2) the auxiliary task of distance map estimation captures the shape better than the contour extraction. Some sample images showing Hausdorff distance for various cases can be seen in Fig. 3.

3) *Segmentation around boundaries*: In the above paragraphs, we have mentioned that our network produces segmentation masks with smooth boundaries. Smooth boundaries indicate a better segmentation around the boundary. We evaluated the segmentation accuracy around boundary with the method adopted in [11]. Specifically, we count the relative number of misclassified pixels within a narrow band (trimap) surrounding actual object boundaries, obtained from the accurate ground truth images. As can be seen in Figure 4, our method has less error for trimaps of different widths.

4) *Visualization of decoder outputs*: Visualising the output maps obtained using the network 1Enc 3Dec MCD will be helpful in understanding how the auxiliary tasks conducted using parallel paths refines the actual segmentation mask.

- In Fig 5, the contour prediction from the contour decoder and the mask prediction from the mask de-

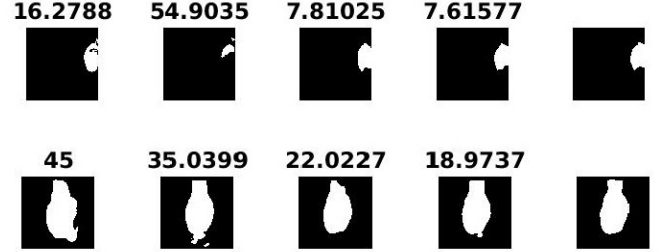


Fig. 3. Hausdorff Distance measures for each model. From left to right : Predicted mask of [2], [3], [4], Ours and Ground Truth Mask.

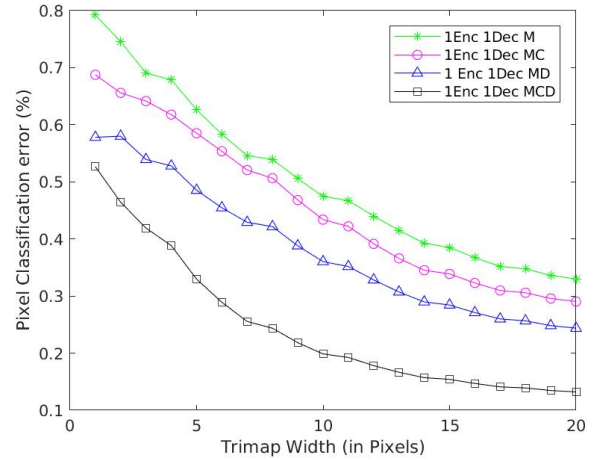


Fig. 4. Percent of misclassified pixels within trimaps of different widths.

coder are taken and compared with their respective ground truths. It is clear that the obtained contours and masks are very close to their respective ground truth. Along with this, another important thing to note is the connection between the predicted mask and contours. The predicted contour can be obtained by finding the perimeter of the predicted mask. Similarly, the predicted mask can be obtained by finding the region filled version of predicted contour.

- In Fig 6, the estimated distance map from the distance decoder and predicted mask from the mask decoder are taken and compared with their respective ground truths. It is clear that the obtained distance map and mask are near to their respective ground truths. Since distance map estimation is a regression task, the distance map will not be equal pixel-wise, but the error between the predicted and ground truth distance map will be less.

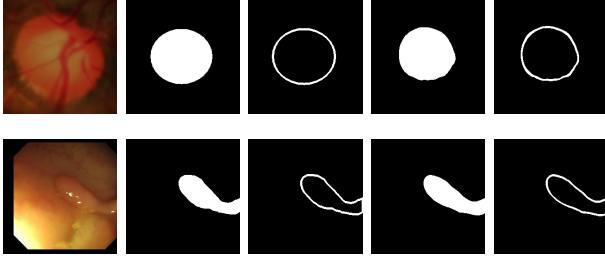


Fig. 5. From left to right: Image, Ground truth mask, Ground truth contour, Predicted mask, Predicted contour.

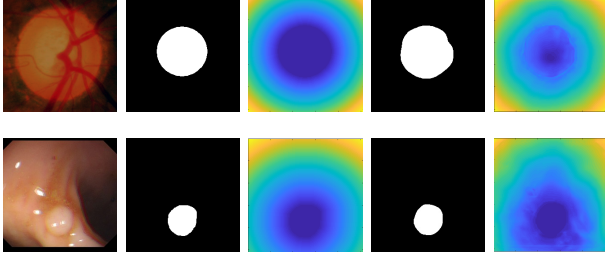


Fig. 6. From left to right : Image, Ground truth mask, Ground truth distance map, Predicted mask, Predicted distance map.

Similar to the relation between mask and contour, a connection between mask and distance map exists. The segmentation map can be obtained from the predicted distance map with a specific threshold. Similarly, the distance map can be obtained from the segmentation map through euclidean distance transform.

This functional relation between mask, contour and distance shows that all the tasks contribute to the final output.

5) *Qualitative comparison:* The qualitative comparison of our network 1Enc 3Dec MCD with 1Enc 1Dec M, 1Enc 2Dec MC and 1Enc 2Dec MD can be seen in Fig. 7. To better appreciate the improvement of our model we have shown only the polyp dataset outputs. The mask predicted by our network and 1Enc 2Dec MD is smooth without outliers

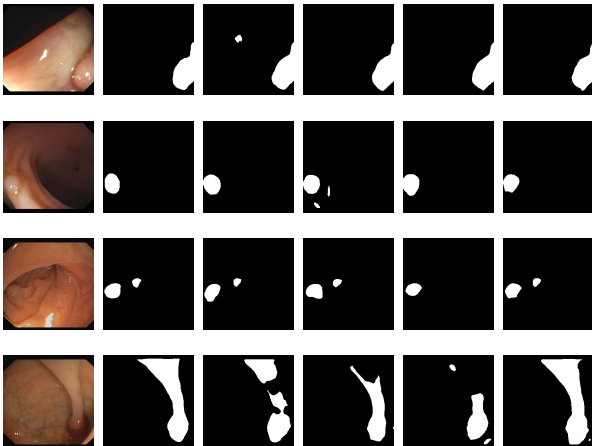


Fig. 7. From left to right : Image, Ground truth mask, Predicted mask of [2], [3], [4] and Ours.

compared to the mask predicted by the networks 1Enc 1Dec M and 1Enc 2Dec MC. This is depicted in the first two rows of the figure. In the third row of the figure, it can be seen that the network 1Enc 1Dec MD fails in case of multi-instance object segmentation while our network performs well as that of 1Enc 2Dec MC. The fourth row shows a case where our network outperforms the other networks.

#### IV. CONCLUSION

In this paper, we have introduced a network called Psi-Net with a single encoder and three parallel decoders. The three decoders are used for mask prediction, contour extraction and distance estimation respectively. We have also introduced a joint loss function to optimize the proposed network. We have shown that this kind of architecture preserves shape well with better boundary outputs and improved segmentation performance.

#### REFERENCES

- [1] G. Litjens, T. Kooi, B. E. Bejnordi, A. A. A. Setio, F. Ciompi, M. Ghafoorian, J. A. W. M. van der Laak, B. van Ginneken, and C. I. Sánchez, "A survey on deep learning in medical image analysis," *Medical Image Analysis*, vol. 42, pp. 60–88, 2017.
- [2] O. Ronneberger, P. Fischer, and T. Brox, "U-Net: Convolutional Networks for Biomedical Image Segmentation," in *Medical Image Computing and Computer-Assisted Intervention – MICCAI 2015*. Springer International Publishing, 2015, pp. 234–241.
- [3] H. Chen, X. Qi, L. Yu, and P. Heng, "DCAN: Deep Contour-Aware Networks for Accurate Gland Segmentation," in *2016 IEEE Conference on Computer Vision and Pattern Recognition (CVPR)*, Jun 2016, pp. 2487–2496.
- [4] C. Tan, L. Zhao, Z. Yan, K. Li, D. Metaxas, and Y. Zhan, "Deep multi-task and task-specific feature learning network for robust shape preserved organ segmentation," in *2018 IEEE 15th International Symposium on Biomedical Imaging (ISBI 2018)*, Apr 2018, pp. 1221–1224.
- [5] F. Milletari, N. Navab, and S. Ahmadi, "V-Net: Fully Convolutional Neural Networks for Volumetric Medical Image Segmentation," in *2016 Fourth International Conference on 3D Vision (3DV)*, Oct 2016, pp. 565–571.
- [6] Z. Mirikharaji and G. Hamarneh, "Star shape prior in fully convolutional networks for skin lesion segmentation," in *Medical Image Computing and Computer Assisted Intervention – MICCAI 2018*. Springer International Publishing, 2018, pp. 737–745.
- [7] S. M. M. R. Al Arif, K. Knapp, and G. Slabaugh, "Shape-aware deep convolutional neural network for vertebrae segmentation," in *Computational Methods and Clinical Applications in Musculoskeletal Imaging*. Springer International Publishing, 2018, pp. 12–24.
- [8] S. M. Shankaranarayana, K. Ram, K. Mitra, and M. Sivaprakasam, "Joint optic disc and cup segmentation using fully convolutional and adversarial networks," in *Fetal, Infant and Ophthalmic Medical Image Analysis*. Springer, 2017, pp. 168–176.
- [9] Z. Zhang, F. S. Yin, J. Liu, W. K. Wong, N. M. Tan, B. H. Lee, J. Cheng, and T. Y. Wong, "Origa-light: An online retinal fundus image database for glaucoma analysis and research," in *Engineering in Medicine and Biology Society (EMBC), 2010 Annual International Conference of the IEEE*. IEEE, 2010, pp. 3065–3068.
- [10] D. Vázquez, J. Bernal, F. J. Sánchez, G. Fernández-Esparrach, A. M. López, A. Romero, M. Drozdal, and A. Courville, "A benchmark for endoluminal scene segmentation of colonoscopy images," *Journal of healthcare engineering*, vol. 2017, 2017.
- [11] P. Krähenbühl and V. Koltun, "Efficient inference in fully connected crfs with gaussian edge potentials," in *Advances in Neural Information Processing Systems 24*, J. Shawe-Taylor, R. S. Zemel, P. L. Bartlett, F. Pereira, and K. Q. Weinberger, Eds. Curran Associates, Inc., 2011, pp. 109–117.